Topic Introduction

Digital Scanned Laser Light Sheet Fluorescence Microscopy

Philipp J. Keller and Ernst H.K. Stelzer

INTRODUCTION

Modern applications in the life sciences are frequently based on in vivo imaging of biological speci-
mens, a domain for which light microscopy approaches are typically best suited. Often, quantitative
information must be obtained from large multicellular organisms on the cellular or even subcellular
level and with a good temporal resolution. However, this usually requires a combination of conflicting
features: high imaging speed, low photobleaching, and low phototoxicity in the specimen, good
three-dimensional (3D) resolution, an excellent signal-to-noise ratio, and multiple-view imaging capa-
bility. The latter feature refers to the capability of recording a specimen along multiple directions,
which is crucial for the imaging of large specimens with strong light-scattering or light-absorbing
tissue properties. An imaging technique that fulfills these requirements is essential for many key
applications: For example, studying fast cellular processes over long periods of time, imaging entire
embryos throughout development, or reconstructing the formation of morphological defects in
mutants. Here, we discuss digital scanned laser light sheet fluorescence microscopy (DSLM) as a novel
tool for quantitative in vivo imaging in the post-genomic era and show how this emerging technique
relates to the currently most widely applied 3D microscopy techniques in biology: confocal fluores-
cence microscopy and two-photon microscopy.

RELATED INFORMATION

The power of advanced in vivo imaging technology is illustrated by the use of fast fluorescence
microscopy to study the dynamics of embryonic development (Vermot et al. 2008). Techniques
that facilitate the imaging of large specimens with strong light-scattering or light-absorbing tissue
properties are described by Huisken et al. (2004), Swoger et al. (2007), and Keller et al. (2008a).

OVERVIEW

DSLM belongs to the family of light-sheet-based fluorescence microscopy (LSFM). In contrast to
conventional and confocal epifluorescence microscopes, which employ the same lens for fluorescence
excitation and detection, LSFM relies on the principle of sample illumination with a planar light sheet
perpendicular to the axis of fluorescence detection (Siedentopf and Zsigmondy 1903; Voie et al.
1993). Optical sectioning arises from the overlap between the focal plane of the fluorescence
detection system and the excitation light sheet (Fig. 1).

Conventional, as well as confocal epifluorescence, microscopes excite fluorophores along the
entire common illumination/detection axis. Hence, when recording a single plane, they cause photo-
bleaching and photodamage everywhere in the specimen (Pawley 2006). The 3D resolution of con-
focal fluorescence microscopes is achieved by discriminating against the light that is emitted outside
the focal plane. In contrast, LSFM provides optical sectioning directly: Fluorophores are only excited
in the illuminated plane, and thus photobleaching and other photoinduced damages are completely
avoided outside the thin volume of interest (Fig. 1). Thereby, LSFM greatly reduces phototoxic effects
(Keller et al. 2007), which actually cause problems in all experiments that rely on imaging. This
circumstance provides LSFM with a decisive advantage in the fast imaging of sensitive biological

www.cshprotocols.org
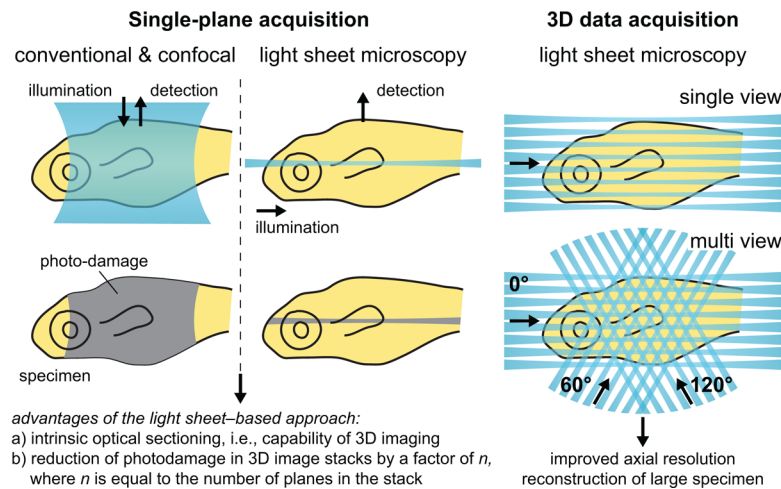
FIGURE 1. Principles of light sheet-based microscopy. (*Left*) Comparison of sample illumination and fluorescence detection in conventional/confocal microscopy and in LSFM. Almost the entire specimen is illuminated in conventional/confocal microscopy, although fluorescence from only a single plane in the specimen is being detected. In contrast, no photodamage is inflicted outside the in-focus plane of the detection system in the light-sheet-based microscope. (*Right*) Three-dimensional imaging in light-sheet-based microscopy is performed by moving the specimen through the light sheet in small steps and recording a two-dimensional image at each step. In DSLM, 3D imaging can alternatively be performed by moving the light sheet through the specimen and by displacing the detection lens accordingly. In multiple-view (or multi view) imaging, the same volume inside the specimen or even the entire specimen is recorded along several angles. The resulting multiple-view information can be combined into a single image stack by data post-processing using a fusion algorithm.

specimens, as well as in in vivo imaging over long periods of time (see Fig. 2A; Arnaout et al. 2007; Keller et al. 2007, 2008a,b; Scherz et al. 2008).

In DSLM, a light sheet is generated with a laser scanner that rapidly moves a micrometer-thin beam of laser light vertically through the specimen (Keller et al. 2008a). The specimen is positioned in front of a second lens, the fluorescence detection lens, and typically embedded in an aqueous gel (Huisken et al. 2004) or in a transparent plastic compartment (Keller et al. 2006). Because of the scanning approach, each line in the specimen is illuminated with the same intensity, which turns DSLM into an excellent tool for the quantitative analysis of large specimens in their entirety. DSLM, furthermore, uses an illumination lens with a low numerical aperture (NA), considerably lower than the NA of the detection lens, which results in a good penetration depth. A further increase in information content can be obtained by observing the same specimen along different directions (see Fig. 2B). Thereby, parts of the specimen become visible that would otherwise be hidden or obscured in the observation along a single direction (Swoger et al. 2007).

THE COMPONENTS OF A DSLM

A DSLM consists of six subsystems (Fig. 3): (1) a light source, (2) a beam-shaping device, (3) a scanning illumination/excitation system, (4) a specimen translating/rotating device, (5) a (multichannel) detection system, and finally (6) the electronics, electrical devices, computer, and software. In contrast to standard fluorescence microscopes (e.g., conventional or confocal fluorescence microscopes), which use the same objective lens for excitation and emission detection (epifluorescence), the DSLM excitation and fluorescence emission collection systems are operated independently. The complete DSLM illumination/excitation system (subsystems 1-3 above; see also Fig. 4) consists, for example, of a multiline argon-krypton laser (e.g., Melles Griot, 35 LTL 835-230), an acousto-optical tunable filter ([AOTF], e.g., AA Opto-Electronic, AA.AOTFnC-400-650-nm-PV-TN) for laser wavelength selection and intensity control, a two-axis high-speed scan head (e.g., GSI Group Lumonics, VM500+), an f-θ lens (e.g., Sill Optics, S4LFT0061/065), and a low-NA illumination objective lens (e.g., Zeiss, Plan-Apochromat 5X/0.16) operated with a regular tube lens. The illumination/excitation objective lens is mounted on a piezo-nanofocus (e.g., Physik Instrumente, P-725.CLQ), which can move the lens up to
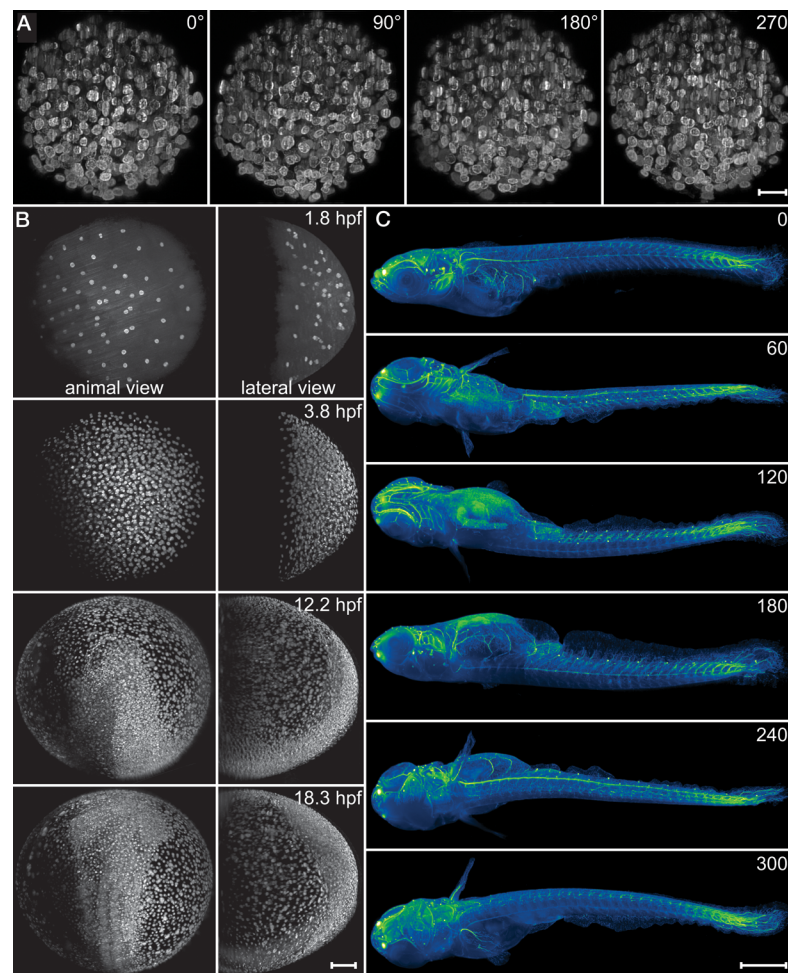
FIGURE 2. Live imaging of embryonic development and multiple-view image acquisition of large multicellular specimens with light-sheet-based microscopy. (*A*) SPIM maximum-intensity projections of a multiple-view data set, showing a spheroid of BXPC-3 pancreas adenocarcinoma cells (obtained with hanging drop method), embedded in 0.5% agarose (~800 cells, diameter ~135 μm). Each projection is based on 310 images. Draq5 nuclear staining (excitation at 633 nm). The SPIM recordings were acquired using a Carl Zeiss Achroplan 40X/0.8 W detection lens and were subsequently deconvolved using the Lucy-Richardson algorithm (20 iterations). Scale bar, 20 μm. Sample by M. Löhr (The German Cancer Research Center [DKFZ]); recording by F. Pampaloni (The European Molecular Biology Laboratory [EMBL]) and M. Marcello (DKFZ). (*B*) DSLM maximum-intensity projections of the animal hemisphere of a wild-type zebrafish embryo showing fluorescence obtained from a nuclear marker (H2B-eGFP provided as mRNA, injection at the one-cell stage). The panels on the *right* show lateral projections of the 3D image stacks (200 images each). The DSLM recordings were acquired using a Carl Zeiss C-Apochromat 10X/0.45 W detection lens and were subsequently deconvolved using the Lucy-Richardson algorithm (10 iterations). Scale bar, 100 μm. Recording in collaboration with A. Schmidt and J. Wittbrodt (EMBL). (*C*) DSLM maximum-intensity projections of a multiple-view data set, showing a 5-mm-long Medaka juvenile with acetylated tubulin immunostaining, providing a view of the fish's nervous system. Six out of 24 angles are shown, using a green/blue lookup table. Each projection is based on 2000 images. The images were acquired using a Carl Zeiss Plan-Neofluar 2.5X/0.075 air lens. Scale bar, 500 μm. Recording in collaboration with A. Schmidt, L. Centanin, and J. Wittbrodt (EMBL). (For color figure, see doi: 10.1101/pdb.top78 online at www.cshprotocols.org.)

400 μm along its optical axis. The specimen is placed inside a custom specimen chamber made, for example, from inert black Delrin. The specimen chamber features a temperature-control system, which includes a temperature sensor inside the chamber and a heating foil attached below the chamber. Custom feedback electronics provide temperature control with a stability of ±0.2°C over several days.

The DSLM detection system (Fig. 4) can take advantage of several detection objective lenses (e.g., from Zeiss, Plan-Neofluar 2.5/0.075, Fluar 5X/0.25, C-Apochromat 10X/0.45 W, Plan-Apochromat 20X/1.0 W, or Plan-Apochromat 63X/1.0 W) mounted on a second independently operated piezo-nanofocus, a beam-splitter cube with exchangeable long-pass filters (e.g., from AHF,
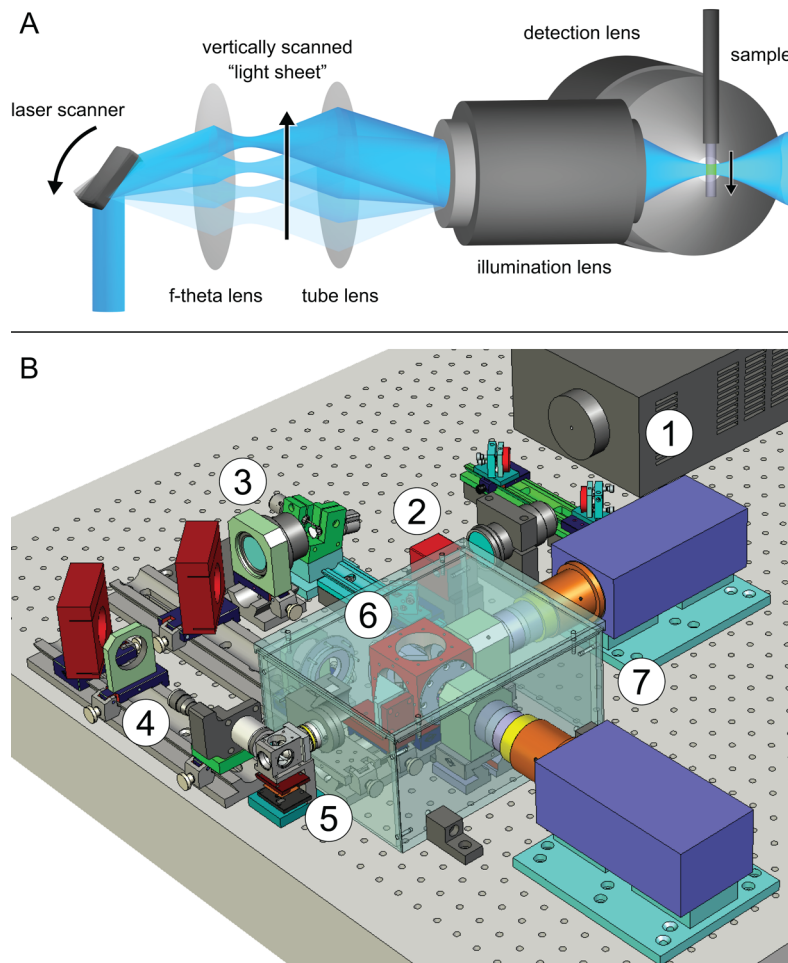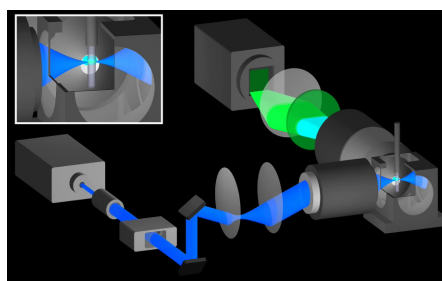
FIGURE 3. The DSLM. (*A*) The laser beam illuminates the specimen from the side and excites fluorophores along a single line. Rapid scanning of a thin volume and fluorescence detection at a right angle to the illumination axis provides an optically sectioned image (Movie 1). The f-θ lens converts the tilting movement of the scan mirror into a vertical displacement of the laser beam. The tube lens and the illumination objective focus the laser beam into the specimen, which is positioned in front of the detection lens. (*B*) Schematic of the central optomechanics of the microscope, including (*1*) the laser-light source, (*2*) the AOTF, (*3*) the laser scanner with the f-θ lens, (*4*) the line-like laser beam illumination arm, (*5*) the temperature-controlled specimen chamber, (*6*) the detector housing with a beam-splitter cube, and (*7*) two wide-field fluorescence detection arms with independently operated cameras. (For color figure, see doi: 10.1101/pdb.top78 online at www.cshprotocols.org.)

Q 565 LP; from Semrock, RazorEdge RU 488 LP, RU 568 LP, or RU 647 LP) and two detection tubes, equipped with two tube lenses and at least two cameras (e.g., the pco.2000 charge-coupled device [CCD] camera from PCO AG). In this implementation, the DSLM detection system records images with a dynamic range of ~10,000 gray levels (i.e., 14 bits) at a maximum speed of 15 frames/sec and per camera and a full CCD image size of 2048 × 2048 pixels (using two analog-to-digital [A/D] converters). Thus, the data rate generated by the dual-channel detection system is 240 MB/sec at maximum speed (126 million pixels/sec). For highest-quality recordings with a single A/D converter per camera, the maximum recording speed of the DSLM-detection system reduces to 63 million pixels/sec (120 MB/sec).

To enhance its ease of use, our DSLM provides a secondary observation system based on a modified pivoting stereo microscope (Zeiss, Stemi 2000-C) equipped with, for example, an infrared light source in the camera port for transmission illumination. The user can pivot the stereo microscope to focus on the center of the DSLM specimen chamber, while simultaneously adjusting the specimen position via the DSLM control software and observing the camera image in the primary fluorescence

MOVIE 1. Schematic operation principle of DSLM. The movie shows a schematic illustration of specimen illumination and fluorescence light detection in the standard DSLM imaging mode. The laser beam illuminates the sample from the side and excites fluorophores along a single line inside the specimen. A pair of laser scanners moves the excitation laser line vertically and horizontally. An optically sectioned image is recorded by rapidly scanning an entire plane in the specimen and detecting the fluorescence at a right angle to the illumination axis. The *top-left inset* shows a zoom-in on the illuminated fraction of the specimen, which is embedded in an agarose cylinder and placed inside the specimen chamber. (To view movie, see doi: 10.1101/pdb.top78 online at www.cshprotocols.org.)

and/or transmission detection system. The direct observation using the stereomicroscope simplifies and speeds up specimen positioning and specimen orientation for optimal DSLM-imaging conditions in the primary detection system (thereby also minimizing the energy load on the specimen).

The illumination and detection subsystems are complemented by a specimen-positioning system, composed of a set of three linear translation stages (Physik Instrumente, M-111K028) and one micro-rotation stage (Physik Instrumente, M-116.DG). The rotation stage with its customized port provides connectors for anodized aluminum specimen holders that hold glass capillaries and plastic syringes.

The operating computer for our DSLM implementation provides four central processing units (CPUs, Intel, Core 2 Quad Q6600 2.4 GHz). The operating software uses two physical CPUs exclusively for the communication with the two camera pipelines, while the remaining two CPUs handle the graphical user interface, subroutines for real-time image processing, and the communication with the main electronics hub. The mass storage device is a high-performance hardware RAID (redundant array of independent disks) controller (Promise, SuperTrak EX8350) with two RAID-0 dual-disk arrays (one per camera), each with 1.5 terabyte (TB) of disk space. The recorded images are written in an alternating manner for the independent RAID systems, thereby doubling the maximum manageable data rate and allowing for operation of the dual-camera detection system at the speed limit of the cameras' A/D converters. Dual-camera data transfer is facilitated via a dual Camera Link controller card (National Instruments, PCIe-1430), installed in the acquisition computer. The other electronics controller cards are located in the DSLM electronics hub, which is attached to the computer via an Ethernet-linked bus extender (Hartmann Elektronik, StarFabric Bridge). The electronics hub includes the scan controller (GSI Group, Lumonics, HC/3), a four-channel stage controller (Physik Instrumente, C-843.41), two multichannel input/output controllers (National Instruments, PCI-6733), and the custom mainframe relay system. The AOTF beam control unit (AA Opto-Electronic, AA.MOD.8C-C**-75.158.24VDC) with an independent linear power supply (Kniel, CA 24.2,5), the dual-channel scanner drivers (GSI Group, Lumonics, MiniSAX) with dedicated linear power supplies (Kniel, CA 15.4), and the custom environmental control system for the specimen chamber are in a separate crate.

We developed custom control software for microscope operation. The programming language C# was used for the user interface and the high-level control layers, and the programming language C++ was used for lower-level hardware communication.

THE DSLM ILLUMINATION SYSTEM

One of the fundamental novel ideas of the DSLM concept is the use of laser scanners to create a two-dimensional sample illumination profile perpendicular to the detection axis. In the standard mode of DSLM operation, one of the scan mirrors of the scan head moves at a constant speed within a predefined angular range. An f-θ lens converts the angular scan range of the laser beam into a vertical set of parallel beams. Because of the scanning approach, a single diffraction-limited beam of light
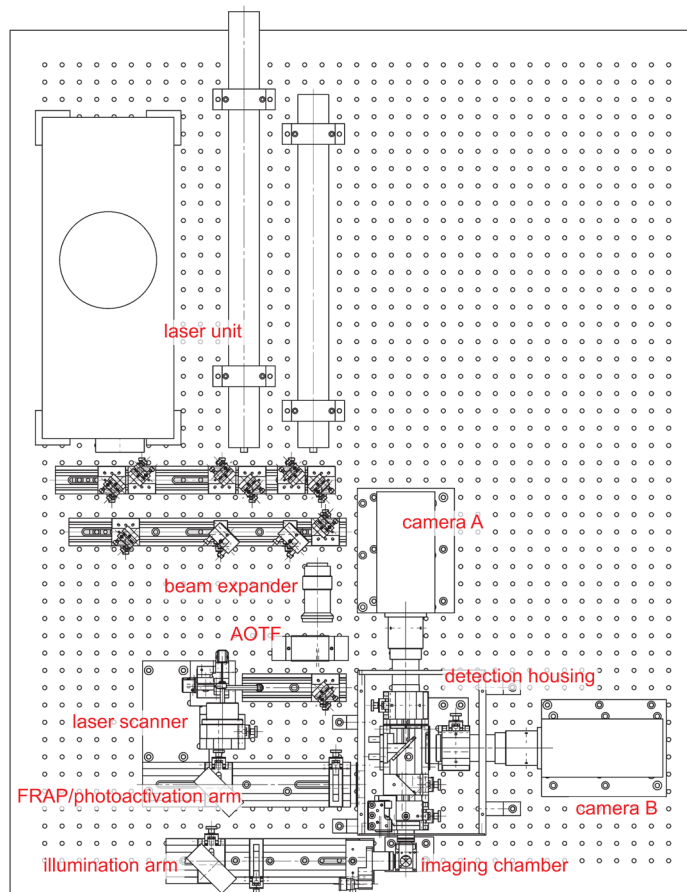
FIGURE 4. Technical blueprint of the DSLM. The technical blueprint shows the complete instrument, as described in the section "The Components of a DSLM." Additional lasers and beam expanders can be added to the illumination system, which provide additional excitation wavelengths and further control over the light sheet thickness. FRAP: Fluorescence recovery after photobleaching.

illuminates the sample at any time point along a well-defined line in space. Integration over time and space results in the illumination of an entire plane. Thus, to obtain a two-dimensional image, the camera integrates the signal while the laser scanners illuminate the respective plane in the detection system's field of view. By using a constant scan speed, a homogeneous light-sheet-like profile is generated (i.e., all horizontal lines are illuminated with the same light intensity). Because of the high scan speed, the entire two-dimensional profile can be created within <1 msec, irrespective of the extent of the field of view.

At any time point during the illumination process, the entire laser intensity (as determined by the setting of the AOTF) is focused into a single diffraction-limited line. In previous light sheet microscope implementations (e.g., single plane illumination microscopy [SPIM]), apertures are necessary to shape the intensity profile (resulting in an average illumination efficiency of 3%). In contrast, the DSLM illumination efficiency of 95% is only limited by the losses at the mirrors and lenses, which amount to considerably <1% per surface (and <5% in total). In addition to the high illumination efficiency, the scanning approach provides a precise control over the vertical extent of the illumination profile.

THE DSLM DETECTION SYSTEM

The main features of the DSLM detection system are (1) a quasi-parallelized detection concept that uses two cameras simultaneously, (2) the possibility of avoiding moving elements such as shutters or filter wheels, (3) cameras with a very large field of view, (4) a minimal number of optical elements, and (5) an electronics concept that allows us to independently address all components digitally and in parallel. In combination, these features maximize the imaging speed.

The detection objective lens is positioned such that its focus overlaps with the light sheet generated by the illumination/excitation system (i.e., the DSLM detection axis is oriented perpendicular to the illumination plane). Each DSLM detection arm consists of a light-insulated tubing system with a tube lens and a camera. To prevent the formation of a dust layer on the protective glass of the camera, both the tube lens and the camera are directly attached to the metal tube cylinder. The fluorescence light collected by the detection objective lens is either transmitted or deflected by 90° at the central detection beam splitter. The beam splitter is optimized for maximum detection efficiency in double-marker experiments that generate fluorescence emission in the channels 488-568 nm and ≥568 nm (e.g., green fluorescent protein [GFP] and tdTomato). The fluorescence light emitted by the first marker is transmitted by the first tube system, whereas the photons emitted by the second marker are deflected toward the second tube system. The beam splitter can be removed to obtain the maximum amount of light in single-channel experiments.

The cameras are triggered asynchronously by the operating software. In the two-channel DSLM recording mode, the two laser wavelengths required to excite the fluorescent marker molecules are activated sequentially. Ideally, while one camera records the signal of the molecules excited with the active laser line, the other camera transfers its data from the previous illumination cycle. Because the electronic downtimes of currently available CCD cameras, due to A/D-converter readout and data transfer (>60 msec), are typically the main limitation in the recording speed, the asynchronous two-channel recording mode effectively doubles the DSLM acquisition rate. As an additional benefit, the concept of alternating acquisitions supersedes the need for spectral unmixing of the two fluorescence signals. Our preferred strategy for specimens with two labels is to excite each fluorophore separately with the optimal wavelength. The fluorescence emission is then observed independently for each fluorophore in a filter arrangement that is optimized for the observation of exactly these two dyes. Our setup would also allow us to excite two dyes at the same time using two or more laser lines and then split the emission with appropriate filters and record the images in parallel. However, the filter requirements become strict, and considerable amounts of energy would not reach the detector. The loss in energy would have to be compensated by longer recording times to achieve an acceptable signal-to-noise ratio.

COMPARISON OF DSLM TO CONVENTIONAL, CONFOCAL, TWO-PHOTON, AND OTHER LIGHT-SHEET-BASED MICROSCOPES

Illumination Efficiency

In DSLM, the entire laser intensity is focused into a single diffraction-limited beam of light, which illuminates the in-focus region of the specimen. Because no apertures are necessary to shape the intensity profile, the DSLM illumination efficiency is almost 100%. The total losses at mirrors and lens surfaces amount to <5%.

In contrast, the illumination efficiency of SPIM is, on average, only 3%. This substantial loss in illumination efficiency (not in detection efficiency) is mainly caused by a set of horizontal and vertical slits that are required to crop the laser profile. The openings define the height and the thickness of the light sheet. This loss occurs both in high-magnification (40X-100X) and in low-magnification (1X-10X) experiments. In high-magnification SPIM experiments, a high illumination NA is required to obtain a thin light sheet (i.e., the thin laser beam has to be expanded). However, because the detected field is very small as a result of the high magnification, the laser profile must subsequently be severely cropped along the vertical dimension. Similarly, in low-magnification SPIM experiments, a low illumination NA is required to obtain a reasonably homogeneous light sheet, but the laser beam has to be expanded to illuminate the large detection field. To reduce the NA, the laser profile must, therefore, be cropped along the horizontal dimension. In conclusion, using the same light source, DSLM records images considerably faster in specimens with a low fluorescence yield (e.g., due to weak staining). Compared with SPIM, a factor of 30 times more fluorescence light is obtained from the sample in the same time interval with a DSLM. Another major advantage is that the power requirements for the DSLM light source are much lower than for the SPIM light source. This allows one to use cheaper, simpler, lower-power, and smaller lasers (i.e., gives access to a much broader range of lasers).

Confocal fluorescence microscopes perform optical sectioning by discriminating against out-of-focus light with the detection pinhole. The detection of the signal from a single plane requires the entire sample to be illuminated. Fluorescence light that is emitted from out-of-focus regions (the majority of the signal) is simply blocked by the detection pinhole. Depending on the imaging

depth within the sample, the confocal fluorescence microscope's illumination efficiency is relatively low. Two-photon fluorescence microscopes are more efficient than confocal fluorescence microscopes because a selection criterion is introduced by the probability density function of the two-photon excitation process. Only the specimen's fluorophores close to the focal region are excited (Denk et al. 1990).

Photobleaching

To achieve the same integrated intensity on the camera chip, DSLM and SPIM deposit the same amount of electromagnetic energy in the specimen. Both microscopy techniques perform optical sectioning by illuminating single planes in the sample at a right angle to the detection system. Whereas SPIM illuminates the entire plane with a constant illumination power, DSLM illuminates the plane section by section. It should be noted that the thickness of the illumination beam spans several lines in the camera and does not necessarily correspond to a single line or less in a camera. For example, at 10X magnification and a CCD pixel pitch of 7.4 µm, a DSLM section corresponds to six complete lines on the camera chip (covering a 4-µm stripe of the object plane). The illuminating laser beams have the same power in SPIM and in DSLM. In DSLM, however, the beam is focused into a line (as compared with the sheet in SPIM). The peak illumination power in the specimen is therefore higher in DSLM (e.g., a factor of 170 at 10X magnification or a factor of 40 at 100X, when using a Hamamatsu ORCA camera). The required range of laser powers in the DSLM is typically between 10 µW and 1 mW. At the upper end of this range, we measured a maximum DSLM irradiance level of 2 kW/cm^2 in the focus region of the illumination profile, which is <20% of the semisaturation level of GFP (11 kW/cm^2) (Kubitscheck et al. 2000). In conclusion, even under the least favorable conditions, DSLM still operates in a linear photobleaching regime, and thus the photobleaching rates in SPIM and DSLM are identical.

Because DSLM performs one-dimensional scanning, the time that is available for the light exposure of a single pixel in the image is several orders of magnitude longer than in confocal and two-photon fluorescence microscopes, which employ two-dimensional scanning. For example, during the 50 msec exposure time per image that is applied in our zebrafish experiments, each pixel in a DSLM image is exposed for ~500 µsec. In contrast, confocal and two-photon fluorescence microscopes require pixel dwell times of 5 µsec and less. Therefore, DSLM can afford, at least, a factor of 100 less laser power in the illumination process compared with confocal and two-photon fluorescence microscopes.

A distinct advantage of DSLM and SPIM is that both implementations only illuminate the plane that is also observed. This advantage can be expressed as a factor *n*, which is the total depth of the image stack required by an experiment divided by the light sheet thickness. Because confocal and conventional fluorescence microscopes illuminate the entire specimen when recording single planes, photobleaching rates in conventional fluorescence microscopes are at least a factor of *n* higher than in DSLM. For example, in a typical DSLM recording of zebrafish development, the light sheet thickness is 4-6 µm, and the image stacks are 600 µm deep. Therefore, DSLM photobleaching is a factor of 100-150 lower than in a conventional fluorescence microscope. Compared with confocal fluorescence microscopes, which operate in nonlinear photobleaching regimes (caused by the high laser power), this factor is usually even larger than *n*.

Two-photon fluorescence microscopes require ultrashort high-energy light pulses in the illumination process because of the low two-photon excitation cross section, and therefore they operate in a nonlinear photobleaching regime. In addition, two-photon optical sections exhibit a large overlap, which results in incremental photodamage in 3D imaging. Therefore, DSLM photobleaching rates are also lower than those found in two-photon fluorescence microscopes.

A detailed side-by-side comparison in the context of zebrafish live imaging revealed that the energy load is a factor of 5600 higher in the confocal fluorescence microscope and a factor of 10^6 higher in the two-photon fluorescence microscope, if compared with the DSLM (Keller et al. 2008a).

Lateral and Axial Extents of the Point-Spread Function

The lateral and axial extents of the point-spread functions of confocal-, two-photon, and light-sheet-based fluorescence microscopes are defined by the wavelengths of the excitation/fluorescence light, the NAs of the objective lenses, and, of course, by the signal-to-noise ratio in the image. Because the same objective lenses can be used in all four techniques, the advantage of one technique over another with respect to the lateral resolution in the recorded data is minor. The lateral performance of the

conventional and the light-sheet-based fluorescence microscopes is identical. The confocal fluorescence microscope will perform $1/\sqrt{2}$ better, and the two-photon fluorescence microscope will perform $\sqrt{2}$ worse; that is, the latter will perform even worse than a conventional fluorescence microscope (Stelzer et al. 1994). It is also well known that the confocal fluorescence microscope cannot take advantage of this improved lateral performance because it generally does not provide a sufficient signal-to-noise ratio (Stelzer 1998).

The situation is different for the axial extents of the point-spread functions. The axial extent of the point-spread function of a conventional microscope is simply determined by the depth of focus of the detection objective lens. The axial extent of any optically sectioning fluorescence microscope is related to the depth of focus of the excitation and detection objective lenses. LSFMs perform optical sectioning with a diffraction-limited illumination profile and provide multiple-view capability (i.e., the option to record multiple data sets of a sample along different angles, see above). In single-view experiments with lenses with relatively low NAs, the LSFMs' axial extents of their point-spread functions are mainly determined by the thickness of the illumination profile. However, it is important to note that the illumination and detection systems in LSFM are decoupled. In contrast to conventional and confocal fluorescence microscopies, the lateral and axial extents of the point-spread functions can, in fact, be defined independently. Usually, the NAs of the LSFM illumination profiles are defined such that the profile thickness at the edge of the field is $\sqrt{2}$ larger than the central thickness, which ensures reasonably homogeneous imaging conditions across the full field of view. Hence, axial resolutions are quite similar in SPIM and DSLM. In multiple-view experiments, the axial resolution can be further improved by fusing the information obtained along different recording angles. For some specimens, the fusion of a few angles already leads to an almost isotropic 3D resolution; that is, the considerably lower axial resolution becomes equal to the much better lateral resolution.

In summary, DSLM and SPIM outperform confocal and two-photon fluorescence microscopes for the entire range of detection NAs in multiple-view experiments. In single-view experiments and for NAs up to ~0.6-0.8 (depending on the field of view of the camera), DSLM and SPIM provide an at least 50% better axial extent of the point-spread functions. At higher NAs, DSLM and SPIM still outperform two-photon microscopes, whereas confocal fluorescence microscopes perform better than LSFMs with NAs >0.8 (Engelbrecht and Stelzer 2006).

It is also important to note that the high signal-to-noise ratio in LSFM (see below) renders LSFM images particularly amenable to image deconvolution, providing a further increase in lateral and axial resolutions (Verveer et al. 2007).

Quality and Flexibility of the Illumination Pattern

This comparison concerns DSLM and SPIM microscopes, which realize optical sectioning with thin diffraction-limited illumination profiles. The illumination profile of SPIM is generated by a set of beam-shaping apertures, a cylindrical lens, and an illumination objective lens. In contrast, DSLM illumination employs laser scanners instead of a cylindrical lens. Thus, beam-shaping apertures are not required in DSLM. In fact, the optical components used in a DSLM are identical to those used in a commercial confocal fluorescence microscope. Hence, the quality of the optical components is excellent.

In the standard DSLM illumination mode, a uniform illumination pattern is generated. The laser intensities are identical for all lines of the recorded plane. The quality of the DSLM profile is only influenced by the field properties of the illumination optics. This is in contrast to SPIM, in which a light-sheet profile is created by focusing an initially collimated Gaussian laser beam profile along one dimension with a cylindrical lens. The unfocused dimension retains the collimated beam properties, and thus, for example, the SPIM illumination intensity is different in the periphery of the field than in its center. DSLM is, therefore, better suited for quantitative imaging and the imaging of large specimens. Our current implementation of DSLM ensures a uniform illumination for samples up to 5 mm in height.

The beam-shaping apertures also affect the quality of the illumination beam. In DSLM, the unconstrained laser beam provides a diffraction-limited focal region. In SPIM, slits constrain the vertical and horizontal extents of the light sheet to obtain the desired light sheet thickness and the required light sheet height at the same time (see above). When imaging large specimens in SPIM (>200 µm), the laser beam must be expanded to achieve an acceptable level of homogeneity along the vertical dimension of the field and subsequently must be cropped along the horizontal dimension to reduce the illumination NA. The constraints imposed on the laser profile usually result in side lobes of the SPIM light sheet and increase the diffraction-limited light sheet thickness.

As an additional benefit of the laser-scanning principle, DSLM provides the intrinsic capability of structured illumination and contrast enhancement. The scanning approach provides flexibility in the illumination system and, for example, allows modulating the intensity profile of the illuminating light sheet. An almost arbitrary intensity function can be realized by AOTF modulation and/or modulation of the scanner acceleration profile.

Imaging Speed

DSLM currently provides two independent camera channels. The cameras are triggered in an alternating scheme and acquire images during the electronic downtime periods of the other camera. While one camera processes and transfers an image to the computer, the other camera is exposed. At low exposure times (<50 msec), DSLM records data at essentially twice the frame rate of a single camera. At an exposure time of 200 msec, there is still a 60% increase in the acquisition rate, when operating, for example, the pco.2000 camera with its full-chip area. Importantly, the scanning approach does not introduce a limitation on the acquisition speed because even an object plane of 5×5 mm can be illuminated within 1 msec. Even the currently fastest electron-multiplying CCD cameras that are capable of transferring the image data to the operating computer during imaging require at least a few milliseconds for data readout and data transfer of a well-sampled image ($\geq 512 \times 512$ pixels), and thus the camera speed is the limiting factor in the DSLM acquisition. In fact, for weakly stained samples, the DSLM scanning illumination actually increases the acquisition rate because the laser light is focused into the sample at almost 100% efficiency, and thus, a larger amount of fluorescence light can be generated and collected from the sample during a short time interval.

The DSLM scanning approach provides another intrinsic imaging-speed advantage over SPIM: The two-axis laser scanner in DSLM allows one to create, as well as to displace, the illumination light sheet. Therefore, a specimen can simply be kept at a fixed position while 3D imaging is performed by rapidly moving the light sheet through the specimen and simultaneously displacing the piezo-mounted detection objective. In this manner, the time-consuming acceleration/deceleration cycles of specimen-positioning stages are completely avoided, and high-speed 3D imaging can be performed even with the most fragile specimens.

Confocal and two-photon fluorescence microscopes use two-dimensional scanning for sample illumination and photomultipliers in the detection; that is, the intensity level in the image is determined one pixel at a time. In a typical 512×512 confocal or two-photon scan field, the 262,144 pixels of each image are illuminated sequentially. In contrast, the camera-based DSLM detection system collects intensity data in parallel for six to eight entire lines on the camera chip, constituting ~16,000 pixels of the final image. The parallelized data acquisition provides DSLM with a dramatic speed advantage over confocal and two-photon fluorescence microscopes. At maximum speed, DSLM records 30 images/sec (using two A/D converters per camera), each 2048×2048 pixels in size, corresponding to an acquisition rate of 126 million pixels/sec. State-of-the-art confocal and two-photon fluorescence microscopes record images at a rate of five frames per second (fps) (and at 120 fps for the Zeiss LSM 5 LIVE) at an image size of 512×512 pixels, corresponding to an acquisition rate of 1.3 million pixels/sec (31 million pixels/sec for the Zeiss LSM 5 LIVE). In conclusion, DSLM is a factor of >90 faster than standard confocal and two-photon fluorescence microscopes and still a factor of 4 faster than the LSM 5 LIVE.

As in DSLM, spinning-disk confocal fluorescence microscopes are able to take advantage of the high imaging speed and high quantum efficiency provided by CCD cameras. Unlike in DSLM, however, the high imaging speed in the spinning-disk confocal fluorescence microscope comes at the expense of the signal-to-noise ratio and is furthermore accompanied by imaging artifacts due to light scattering and the loss of incoherence arising from the simultaneous use of multiple pinholes.

Finally, it should be noted that each sample provides a limited photon budget; that is, faster scanning will also inevitably lead to an accordingly increased photobleaching rate. Thus, line-scanning or resonant-scanner confocal microscopy implementations are particularly unsuited for long-term high-speed imaging because of the extremely high photobleaching rates.

Dynamic Range

Both DSLM and SPIM feature camera-based detection and thereby benefit from the high dynamic range of CCDs and other semiconductor-based cameras. The DSLM detection system provides images with a dynamic range of 10,000 gray levels. Confocal and two-photon fluorescence microscopes typically provide data with a dynamic range of at most 6-8 bits (64-256 gray levels). One advantage

of a high dynamic range is the possibility to perform image deconvolution to increase the resolution (Verveer et al. 2007). More importantly, the high dynamic range is very helpful in time-lapse imaging of vertebrate development: For example, in experiments with nuclei-labeled zebrafish embryos, the high dynamic range facilitates a precise quantification of changes in nuclear intensity levels. This information yields the level of DNA compaction and thereby reveals the cell-cycle state, without a need for additional markers.

Cost Efficiency

Our design of DSLM is optimized with respect to the number of components and optical interfaces in the illumination system. Taking into account the number of degrees of freedom that are required to operate the elements in our instrument, we are probably, at most, two elements short of using the minimal number of optical parts. In this sense, DSLM provides an almost optimal solution. We also took particular care to ensure a very compact implementation. The microscope currently has a footprint of 0.3 m^2 on the optical table (excluding the light source). The total price tag for our implementation of DSLM is 80,000 € (excluding the development of software and customized electronics). Using a single camera and reducing the amount of optical components, a DSLM can be built for as little as 50,000 €.

Table 1. Performance comparison of 3D fluorescence microscopy in the context of long-term in vivo imaging of entire embryos

	DSLM	Confocal	Two photon
Sectioning efficiency[a]	In-focus plane	Entire specimen	In-focus plane and surface contribution
Energy load[b]	E	$\sim 10^3 \cdot E$	$\sim 10^6 \cdot E$
Lateral resolution[c]	r	$r/\sqrt{2}$	$r \cdot \sqrt{2}$
Axial resolution[d]	++ (equivalent to lateral resolution in multiview)	+	–
Imaging speed[e]	63 Mvoxel/sec	2-6 Mvoxel/sec	1 Mvoxel/sec
Signal-to-noise ratio[f]	1000:1	60:1	10:1
Cost-efficiency[g]	≥50,000 €	>100,000 €	>200,000 €

++ represents good performance, + represents medium performance, and – represents low performance.

[a]That is, efficiency in using illumination light exclusively for fluorescence excitation in the focal plane of the detection lens; the surface contribution in two-photon microscopy depends on the laser power/depth in the specimen.

[b]Relative factors depend on total embryo size; factors were measured for nuclei-labeled zebrafish embryos (Keller et al. 2008a).

[c]Not considering image deconvolution; with image deconvolution, the DSLM lateral resolution is superior to the lateral resolution of a confocal microscope (Verveer et al. 2007).

[d]Considering DSLM multiple-view capability, exact values depend on the choice of objective.

[e]Only considering implementations that are suitable for long-term high-speed imaging, i.e., no line-scanning confocal microscopes. Also, confocal imaging with resonant scanners reaches a speed of ~6 Mvoxel/sec but is unsuitable for imaging of entire embryos at high spatial resolution, owing to the reduced field size.

[f]Average performance at maximum imaging speed.

[g]Considering costs for additional optical components in confocal and two-photon microscopes as well as the costs for high-performance lasers (in particular, for two-photon microscopes).
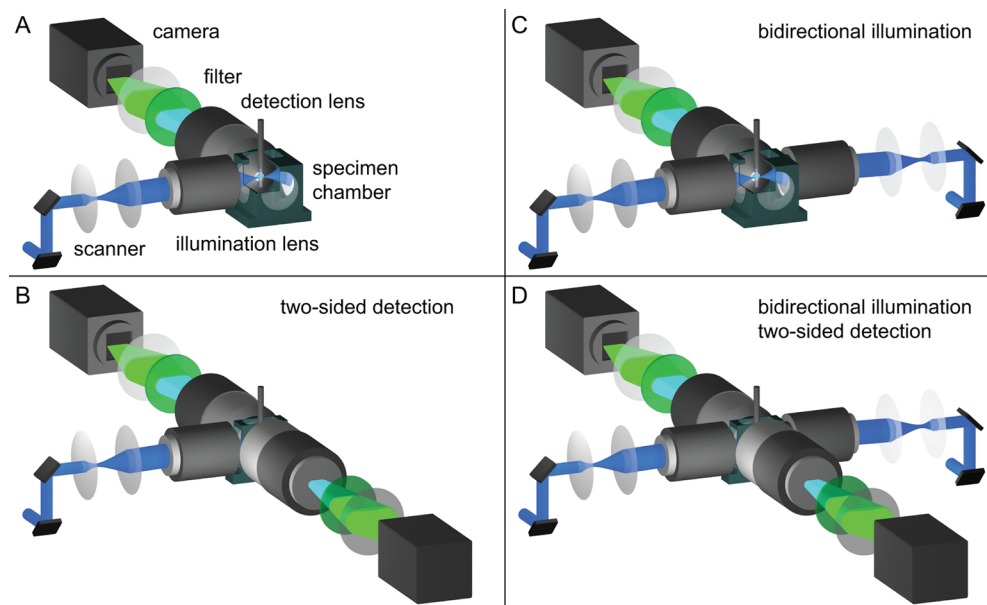
FIGURE 5. Advanced implementations of DSLM. (*A*) Schematics of the standard DSLM implementation, as well as (*B*) extended versions with two-sided detection, (*C*) bidirectional illumination, and (*D*) a combination of both. Multisided illumination typically yields a more homogeneous light exposure in the illumination process, whereas simultaneous multisided detection saves recording time and illumination light energy in multiple-view imaging. (For color figure, see doi: 10.1101/pdb.top78 online at www.cshprotocols.org.)

CONCLUSIONS

DSLM is particularly well suited to address the issues encountered in in vivo imaging of large multicellular organisms. DSLM provides up to 50 times higher imaging speeds and a 10-100 times higher signal-to-noise ratio, while exposing the specimens to at least three orders of magnitude less light energy than confocal and two-photon fluorescence microscopes (Table 1; for color table, see doi: 10.1101/pdb.top78 online at www.cshprotocols.org.).

Further improvement of the technology is possible—for example, by upscaling and parallelizing the laser illumination and fluorescence detection process (Fig. 5). For example, an extension of our current implementation to two-sided specimen illumination is straightforward. Such an extension has been very successfully applied in SPIM and allows for increased illumination homogeneity of large specimens that exhibit low transparency and high light-scattering properties (Huisken and Stainier 2007; Scherz et al. 2008). Likewise, the detection system can be extended by using two cameras with opposing views of the specimen. Such an implementation provides intrinsic multiple-view capability and decreases the recording time required for collecting the fluorescent signal from different directions. A combination of these ideas yields a particularly powerful extension of DSLM with bidirectional line-scanning illumination and two-sided detection.

REFERENCES

Arnaout R, Ferrer T, Huisken J, Spitzer K, Stainier DY, Tristani-Firouzi M, Chi NC. 2007. Zebrafish model for human long QT syndrome. *Proc Natl Acad Sci* **104:** 11316–11321.

Denk W, Strickler JH, Webb WW. 1990. Two-photon laser scanning fluorescence microscopy. *Science* **248:** 73–76.

Engelbrecht CJ, Stelzer EH. 2006. Resolution enhancement in a light-sheet-based microscope (SPIM). *Opt Lett* **31:** 1477–1479.

Huisken J, Stainier DY. 2007. Even fluorescence excitation by multidirectional selective plane illumination microscopy (mSPIM). *Opt Lett* **32:** 2608–2610.

Huisken J, Swoger J, Del Bene F, Wittbrodt J, Stelzer EH. 2004. Optical sectioning deep inside live embryos by selective plane illumination microscopy. *Science* **305:** 1007–1009.

Keller PJ, Pampaloni F, Stelzer EH. 2006. Life sciences require the third dimension. *Curr Opin Cell Biol* **18:** 117–124.

Keller PJ, Pampaloni F, Stelzer EH. 2007. Three-dimensional preparation and imaging reveal intrinsic microtubule properties. *Nat Methods* **4:** 843–846.

Keller PJ, Schmidt AD, Wittbrodt J, Stelzer EH. 2008a. Reconstruction of zebrafish early embryonic development by scanned light sheet microscopy. *Science* **322:** 1065–1069.

Keller PJ, Pampaloni F, Lattanzi G, Stelzer EH. 2008b. Three-dimensional microtubule behavior in *Xenopus* egg extracts reveals four dynamic states and state-dependent elastic properties. *Biophys*

J **95:** 1474–1486.

Kubitscheck U, Kuckmann O, Kues T, Peters R. 2000. Imaging and tracking of single GFP molecules in solution. *Biophys J* **78:** 2170–2179.

Pawley J. 2006. *Handbook of confocal microscopy*. Springer, New York.

Scherz PJ, Huisken J, Sahai-Hernandez P, Stainier DY. 2008. High-speed imaging of developing heart valves reveals interplay of morphogenesis and function. *Development* **135:** 1179–1187.

Siedentopf H, Zsigmondy R. 1903. Über Sichtbarmachung und Größenbestimmung ultramikroskopischer Teilchen, mit besonderer Anwendung auf Goldrubingläser. *Ann Phys* **315:** 1–39.

Stelzer EHK. 1998. Contrast, resolution and the signal to noise ratio in fluorescence microscopy. *J Microsc* **1:** 15–24.

Stelzer EHK, Hell SW, Lindek S, Stricker R, Pick R, Storz C, Ritter G, Salmon N. 1994. Nonlinear absorption extends confocal fluores-cence microscopy into the ultra-violet regime and confines the illumination volume. *Opt Commun* **104:** 223–228.

Swoger J, Verveer P, Greger K, Huisken J, Stelzer EHK. 2007. Multi-view image fusion improves resolution in three-dimensional microscopy. *Opt Express* **15:** 8029–8042.

Vermot J, Fraser SE, Liebling M. 2008. Fast fluorescence microscopy for imaging the dynamics of embryonic development. *HFSP J* **2:** 143–155.

Verveer PJ, Swoger J, Pampaloni F, Greger K, Marcello M, Stelzer EH. 2007. High-resolution three-dimensional imaging of large specimens with light-sheet-based microscopy. *Nat Methods* **4:** 311–313.

Voie AH, Burns DH, Spelman FA. 1993. Orthogonal-plane fluores-cence optical sectioning: Three-dimensional imaging of macro-scopic biological specimens. *J Microsc* **170:** 229–236.